VERSITA

OPTO-ELECTRONICS REVIEW **18**(4), 438–445

DOI: 10.2478/s11772-010-0049-0

Absorption loss influence on optical characteristics of multilayer distributed Bragg reflector: wavelength-scale analysis by the method of single expression

H.V. BAGHDASARYAN*[1], T.M. KNYAZYAN[1], T.H. BAGHDASARYAN[2], B. WITZIGMANN[3], and F. ROEMER[3]

[1]Fiber Optics Communication Laboratory, State Engineering University of Armenia, 105 Terian Str., 0009 Yerevan, Armenia
[2]Optics Department, Yerevan State University, 1 Alex Manoogian Str., 0025 Yerevan, Armenia
[3]Computational Electronics and Photonics Group, University of Kassel, Wilhelmshoeher Allee 71, D-34121 Kassel, Germany

Electrodynamical model of a classical distributed Bragg reflector (DBR) consisting of alternating quarter-wave layers of high and low permittivity is considered at the plane wave normal incidence. Reflective characteristics of DBR possessing absorption loss in constituting layers are analysed via correct wavelength-scale boundary problem solution by the method of single expression (MSE). Analysis of optical field and power flow density distributions within the lossy DBR structures explained the peculiarities of their reflective characteristics. Optimal configurations of lossless and lossy DBRs are revealed. Specific DBR structures possessing full transparency at definite number of layers are also analysed.

Keywords: quarter-wave layers, lossy DBR, transparent DBR, method of single expression (MSE), wavelength-scale analysis, boundary problem solution, optical field distribution.

1. Introduction

Multilayer structure of alternating quarter-wave layers of high and low permittivity known in literature as distributed Bragg reflector (DBR) usually is made of dielectric or semiconductor material. DBRs possess good reflecting properties and they are used as stop-band filters and frequency-selective reflectors in different components of modern fiber-optic communication systems and integrated optics, namely, in vertical-cavity surface-emitting lasers (VCSELs) [1,2], resonant cavity light emitting diodes (RCLEDs) [3,4], resonant cavity enhanced (RCE) photodetectors [5], and surface-normal electro-absorption modulators [6,7]. As active layers of surface-normal operating devices are very thin, then their multilayer mirrors should have high enough reflectance to provide an efficient operation [1–7]. High reflectance of such mirrors is normally attained at great number of layers, which in the case of X-ray and UV multilayer mirrors can reach some hundreds [8,9]. Absorption loss in the layers of multilayer mirrors diminishes their reflectance and in this connection it is important to reveal optimal configuration of DBRs via correct computer modelling before costly fabrication process [10].

An analysis of DBRs by different mathematical methods and their practical application have a long history starting from the early 20th century [8,11–13]. However, there is one aspect of DBRs still expecting clarification, namely the physics of absorption loss influence on DBR reflection. An impact of low absorption loss in layers of DBR on its reflective properties has been analysed previously [13,14]. There is information that reflection of DBR with low loss at infinite number of layers strongly depends on the relative value of permittivity of the first layer. In Ref. 14, this difference in DBRs reflection is explained by a different penetration depth of light in the structure depending on the relative value of first layer's permittivity. However, the physics of this phenomenon continues to be unclear. An importance of analysis of optical field distribution within DBR structures for explanation of loss impact and high intensity optical radiation on its reflective and transmissive properties has been noticed previously [8,15–17]. In the present paper, the physics of loss impact on DBR reflectance is clarified through the detailed analysis of optical field distribution peculiarities within DBR structures.

For detailed analysis of DBRs' optical characteristic several computational methods are in use. Widely used calculation method is the coupled mode theory (CMT) [18–21]. The CMT provides simple analytical expressions also for mirrors having graded interfaces, however, the applicability of the method is limited by DBR structures with low index contrast [22]. The calculation method close to the CMT is the Tanh

*e-mail: hovik@seua.am

substitution technique, which is used to find the reflectance of abrupt and graded multilayer mirrors [23]. In the CMT, the conception of two coupled counter-propagating waves is used instead of correct electrodynamical boundary problem solution. For this reason, the distinction of DBR structures starting and/or ending with high or low permittivity values on the subject of reflection characteristics is impossible. However, as it follows from the analysis carried out in the present paper by the MSE, the relative value of the permittivity of starting and ending layers is crucial parameter for reflective and transmissive properties and absorption loss influence on optical characteristics of DBRs.

Numerical calculation of multilayer structures is generally carried out by the transfer matrix method (TMM) [8,11–13]. The TMM is commonly used in analysing multilayer structures with abrupt interfaces on the subject of DBR reflectance and transmittance. To obtain information on optical field and power flow density distribution within a multilayer structure with respect to loss by the TMM it is necessary to divide each layer of the structure on sufficient number of homogeneous sub-layers. By choosing an appropriate thickness of the sub-layers, it is possible to get information regarding the distribution of optical field and power flow density within the DBR structures.

Powerful computational method is the finite-difference time-domain method (FDTDM) [24] which along with DBRs' reflectance and transmittance is able to provide with the optical field and power flow distribution in the structure. Though FDTDM requires essential computer resources and needs comparatively long time for computation in the case of 3D optical structures, however, it is quite efficient and fast in the case of 1D structures.

In the present paper, to analyse optical characteristics of DBR with absorption loss, an alternative approach to electrodynamical boundary problem solution is used. In this approach, the general solution of Helmholtz equation is presented in the form of a single expression but not in the form of the sum of two counter-propagating waves, as it is widely adopted in the literature. On the basis of this approach, an advanced method, called method of single expression (MSE), has been developed which allows for solving correctly wavelength-scale boundary problems for multilayer and modulated media as well [17,25–29]. The MSE is intrinsically exact method without any mathematical approximations. The MSE is computer-oriented approach and possesses both high accuracy and fast calculation even on common desktop computers that makes it highly suitable for optimisation task solution. No restriction on the value of loss is implied in the MSE. In the following, the main principles of the MSE are presented along with the thorough analysis of DBRs with absorption loss in constituting layers.

2. Main principles of the MSE

Detailed description of the MSE has been presented in Refs. 17, and 25–29. In the following, main principles of the MSE are described.

Starting from Maxwell's equations in 1D case, the following Helmholtz equation can be obtained

$$\frac{d^2\dot{E}_x(z)}{dz^2}+k_0^2\tilde{\varepsilon}(z)\dot{E}_x(z)=0, \tag{1}$$

where $\dot{E}_x$ is the linearly polarised electric field component, $k_0=\omega\sqrt{\varepsilon_0\mu_0}$ is the free space propagation constant, and $\tilde{\varepsilon}(z)=\varepsilon'(z)+i\varepsilon''(z)$ is the complex permittivity of a medium. Equation (1) is applicable not only for homogeneous media when $\tilde{\varepsilon}(z)=const$, but also for any longitudinally inhomogeneous media under the condition $\vec{E}\perp grad\varepsilon$.

The essence of the MSE is the presentation of the general solution of Helmholtz equation in the special form of a single expression

$$\dot{E}_x(z)=U(z)\exp(-iS(z)), \tag{2}$$

instead of traditional presentation as a sum of two counter-propagating waves. Here, $U(z)$ and $S(z)$ are the real quantities describing the resultant electric field amplitude and phase, respectively. MSE is inherently frequency domain approach where the time dependence $\exp(i\omega t)$ is assumed but suppressed throughout the analysis.

The following form the foundation of the MSE:

- presentation of electric field component in the form of a single expression, Eq. (2),
- rewriting Helmholtz Eq. (1) in terms of the variables $U(z)$ and $S(z)$,
- matching boundary conditions of electrodynamics in terms of the variables $U(z)$ and $S(z)$,
- backward numerical calculation algorithm.

Based on Eq. (2), Helmholtz Eq. (1) is reformulated to the set of the first order differential equations regarding the electric field amplitude U(z), its spatial derivative Y(z) and the quantity $P(z)=U^2(z)[dS(z)/d(k_0z)]$ proportional to the power flow density (Poynting vector) in a medium

$$\begin{cases}\dfrac{dU(z)}{d(k_0z)}=Y(z)\\ \dfrac{dY(z)}{d(k_0z)}=\dfrac{P^2(z)}{U^3(z)}-\varepsilon'(z)U(z).\\ \dfrac{dP(z)}{d(k_0z)}=\varepsilon''(z)U^2(z)\end{cases} \tag{3}$$

Poynting vector (the time-averaged power flow density) is expressed as [17]

$$\Pi_z=\frac{1}{2}\mathrm{Re}[\dot{E}_x(z)\dot{H}_y(z)]=\frac{1}{2}\sqrt{\frac{\varepsilon_0}{\mu_0}}P(z). \tag{4}$$

The sign of $P(z)$ indicates the direction of power flow in a medium, namely, positive value describes power flow along z axis, negative – in opposite direction. Depending on the sign of $\varepsilon''(z)$, it is possible to take into account loss or gain in a medium.

In describing waves outside of the investigated structure, a traditional approach of counter- propagating waves is used. Inside the structure, the form of solution given by Eq.

(2) is used. By imposing boundary conditions of electrodynamics at the borders of the investigated structure, the numerical integration of the set of differential Eq. (3) starts from the non-illuminated side of the structure. Only one outgoing travelling wave exists behind the structure. Initial parameters obtained from the boundary conditions at the non-illuminated side of the structure ($z = L$) are $U(L) = E_{tr}$, $Y(L) = 0$, and $P(L) = U^2(L)\sqrt{\varepsilon_r}$. Here, E_{tr} is the amplitude of transmitted wave and ε_r is the permittivity of a medium behind the structure. Numerical integration of the set of Eq. (3) goes step by step towards the illuminated side of the structure taking into account an actual value of structure's permittivity (both real and imaginary parts) for the given coordinate at each step of integration. At the borders between constituting layers of the multilayer structure, ordinary boundary conditions of electrodynamics bring to the continuity of $U(z)$, $Y(z)$, and $P(z)$.

From the boundary conditions of electrodynamics, at the illuminated side of the structure (at $z = 0$), the amplitude of incident field

$$E_{inc} = \left| \frac{U^2(0)\sqrt{\varepsilon_l} + P(0) + jU(0)Y(0)}{2U(0)\sqrt{\varepsilon_l}} \right|, \qquad (5)$$

and power reflection coefficient

$$R = \frac{E_{ref}^2}{E_{inc}^2} = \left| \frac{U^2(0)\sqrt{\varepsilon_l} - P(0) - jU(0)Y(0)}{U^2(0)\sqrt{\varepsilon_l} + P(0) + jU(0)Y(0)} \right|^2, \qquad (6)$$

are restored at the end of calculation. Here, ε_l is the permittivity of a medium in front of the structure. The power transmission coefficient T of the structure is calculated as $T = (\sqrt{\varepsilon_r}\, E_{tr}^2)/(\sqrt{\varepsilon_l}\, E_{inc}^2)$.

Though a backward direction of boundary problem solution used in the MSE (when the amplitude of incident wave is not given at the start but restored at the end of computation) is not widely accepted, however, it guarantees the uniqueness of solution through a single process of computation without iterations. When the boundary problem solution starts from the illuminated side of the structure, which is natural for other methods, iterations are unavoidable [30].

Solution presentation in the MSE is more general than traditional counter-propagating waves approach, there is no necessity to preset the forms of waves in different media and to satisfy the superposition principle condition. This makes the MSE an effective tool for correct steady-state description of electromagnetic waves interaction with not only linear media (including media with loss or gain) but also with nonlinear media where permittivity is intensity dependent value. An implementation of the MSE for semiconductor and metallic media is straightforward, since material properties of any media can be adequately described by relevant electrodynamical parameters, i.e., *via* real and imaginary parts of permittivity. There are no restrictions on the sign and value of real and imaginary parts of permittivity in any layer of a multilayer structure in the MSE.

3. Numerical results and discussions

3.1. Lossless DBRs at central wavelength

The normal incidence of linearly polarised plane electromagnetic wave on the DBR structure of alternating quarter-wave layers is considered. The wave incidence from the left side of the structure is assumed (Fig. 1).

At the central wavelength λ_{cen}, the condition $\lambda_{cen}/4 = d_L\sqrt{\varepsilon_L} = d_H\sqrt{\varepsilon_H}$ for quarter-wave layers is satisfied. Here, ε_L and ε_H are the low and high permitivities of alternating quarter-wave layers, d_L and d_H are the layers' thickness. In Fig. 2, the permittivity profiles of possible four types of DBR structures with even and odd number of constituting layers are presented.

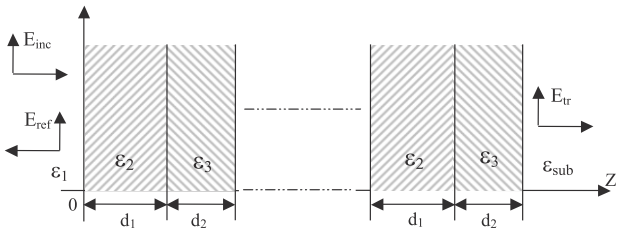

Fig. 1. Normal incidence of plane electromagnetic wave on a multilayer structure consisting of alternating quarter-wave layers on a substrate of the permittivity $\varepsilon = \varepsilon_{sub}$.

The analytical formulae for DBR reflectance are derived only for lossless DBRs for even and odd number of layers [8,11,13,31].

Even number of layers. DBRs consisting of N pairs of quater-wave layers of the permittivity ε_L and ε_H sandwiched between two media of the permittivity ε_1 and ε_{sub} are schematically presented as $\varepsilon_1/(\varepsilon_L/\varepsilon_H)\times N/\varepsilon_{sub}$ [Fig. 2(a)] and $\varepsilon_1/(\varepsilon_H/\varepsilon_L)\times N/\varepsilon_{sub}$ [Fig. 2(b)]. The reflectance R_N at the central wavelength is described by the following formula [8,11,31]

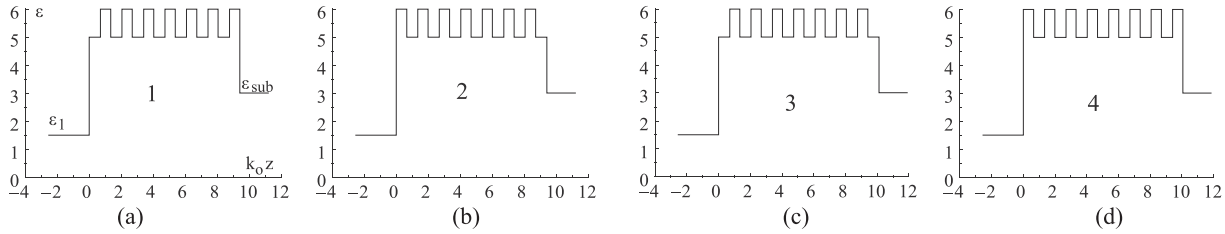

Fig. 2. Permittivity profiles of: DBRs composed of bilayers (even number of layers) starting by ε_L (a) and starting by ε_H (b), DBRs composed of bilayers plus one layer (odd number of layers) starting and ending by ε_L (c) and starting and ending by ε_H (d).

$$R_N = \left(\frac{\sqrt{\varepsilon_1}\varepsilon_3^N - \sqrt{\varepsilon_{sub}}\varepsilon_2^N}{\sqrt{\varepsilon_1}\varepsilon_3^N + \sqrt{\varepsilon_{sub}}\varepsilon_2^N} \right)^2, \quad (7)$$

where $\varepsilon_2 = \varepsilon_L, \varepsilon_3 = \varepsilon_H$ or $\varepsilon_3 = \varepsilon_H, \varepsilon_3 = \varepsilon_L$.

In the case of $\varepsilon_{sub} = \varepsilon_1$, there is no difference in the reflectance R_N for the structures starting from the layer of ε_L or ε_H. However, the distributions of electric field amplitude within these structures are completely different (see Fig. 4) that it has been indicated in Ref. 17.

Odd number of layers. DBRs consisting of N pair of quater-wave layers of the permittivity ε_L and ε_H plus one layer and sandwiched between two media of the permittivity ε_1 and ε_{sub} are schematically presented as $\varepsilon_1/(\varepsilon_L/\varepsilon_H)\times N + \varepsilon_L/\varepsilon_{sub}$ [Fig. 2(c)] and $\varepsilon_1/(\varepsilon_H/\varepsilon_L)\times N + \varepsilon_H/\varepsilon_{sub}$ [Fig. 2(d)]. The reflectance R_{N+1} is described by the following formula [11,13,31]

$$R_{N+1} = \left(\frac{\sqrt{\varepsilon_1}\sqrt{\varepsilon_{sub}}\varepsilon_3^N - \varepsilon_2^{N+1}}{\sqrt{\varepsilon_1}\sqrt{\varepsilon_{sub}}\varepsilon_3^N + \varepsilon_2^{N+1}} \right)^2, \quad (8)$$

where $\varepsilon_2 = \varepsilon_L, \varepsilon_3 = \varepsilon_H$ or $\varepsilon_2 = \varepsilon_H, \varepsilon_3 = \varepsilon_L$.

The reflectance R of the possible four types of lossless DBRs *vs.* the number of bilayers N are plotted in Fig. 3 in accordance with Eqs. (7) and (8). The analysis of the reflectances of DBRs are carried out also by the MSE and an excellent agreement with the analytical results is obtained. For all DBRs at high enough values of N the reflectances R_N and R_{N+1} tend to the saturated value equal to unity. However, at the modest number of bilayers, the reflectances differ essentially.

The structure 4 provides the most drastic increase in the reflectance by increase in the bilayers number N. The character of the dependences presented in Fig. 3 is preserved for any other values of permittivity contrast. At low contrast, the reflectance saturation is observed at great number of bilayers and *vice versa*, at high contrast, the reflectance saturation is observed at low number of bilayers.

For completeness of the analysis, it is desirable to present the distributions of electric field amplitude within the lossless DBR structures. The knowledge of field distribution is useful in predicting an influence of absorption loss in constituting layers of a structure on its reflectance, as well as

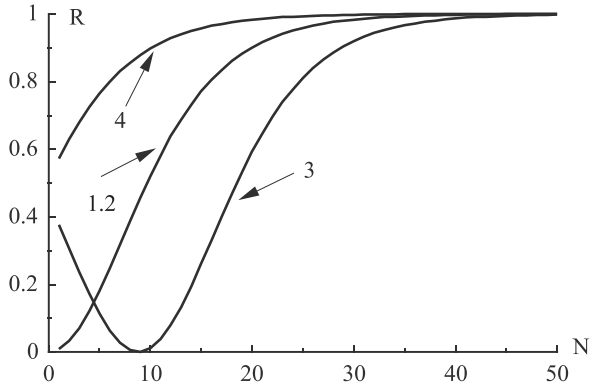

Fig. 3. The reflectances R of four possible types of DBRs on the number of bilayers N. Numeral of a curve corresponds to numbering of DBR in Fig. 2, $\varepsilon_L = 5$, $\varepsilon_H = 6$; and $\varepsilon_1 = \varepsilon_{sub} = 1$.

the stability of the DBR to high intensity optical radiation. The following analysis is carried out by the MSE.

In Fig. 4, the distributions of electric field amplitude for possible four types of DBR structures (presented in Fig. 2) are shown at fixed amplitude of the incident field (E_{inc} = 3 a.u.). In case of linear problem solution, the value of incident field amplitude can be taken as arbitrary one. At any fixed amplitude of the incident field E_{inc}, there are incident power flow density $P_{inc} = E_{inc}^2\sqrt{\varepsilon_1}$ and reflected power flow density $P_{ref} = RP_{inc}$ in front of the structure, the power flow density P_{str} within the structure and the transmitted power flow density $P_{tr} = TP_{inc}$ behind the structure. In Figs. 4, 5, and 7, the resultant power flow density P is indicated, where in front of the structure $P(z<0) = P_{inc} - P_{ref}$. In the considered case, when there are no currents or free charges in the media and interfaces the condition of continuity of power flow density is satisfied. Thus, for each lossless DBR structure, the resultant power flow density P within and outside of the structure (Figs. 4 and 5) is the constant value $P = P_{inc} - P_{ref} = P_{str} = P_{tr}$.

On the illuminated side of the structures (at $z < 0$), partially standing wave pattern is formed in the result of superposition of incident and reflected waves. Though the reflectance is the same for the structures of equal even number of layers (structures 1 and 2), the distributions of electric field amplitude differ strongly within them. The envelopes of electric field amplitude in structure 2 and 4 (starting by

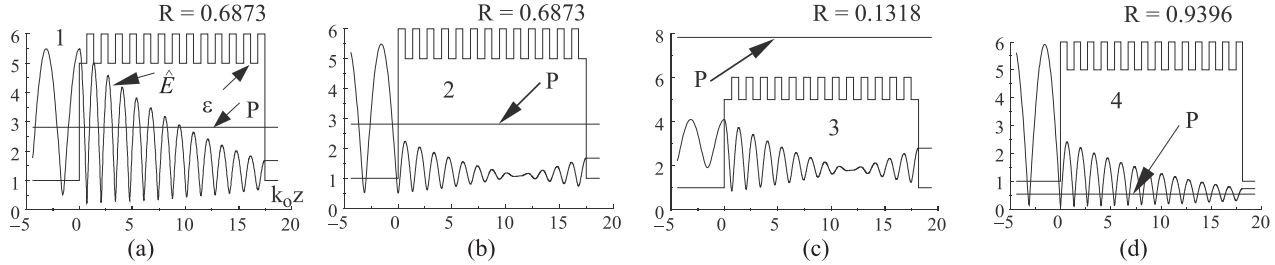

Fig. 4. The permittivity profile, distributions of electric field amplitude $\hat{E}$ and the power flow density **P** in lossless DBRs of the following alternation of the layers: (a) $\varepsilon_1/(\varepsilon_L/\varepsilon_H)\times N/\varepsilon_1$, (b) $\varepsilon_1/(\varepsilon_H/\varepsilon_L)\times N/\varepsilon_1$, (c) $\varepsilon_1/(\varepsilon_L/\varepsilon_H)\times N + \varepsilon_L/\varepsilon_1$, and (d) $\varepsilon_1/(\varepsilon_H/\varepsilon_L)\times N + \varepsilon_H/\varepsilon_1$ at $N = 13$. DBRs are surrounded from both sides by the air $\varepsilon_1 = 1$. Incident field comes from the left of a structure. Corresponding values of the reflectance R are presented.

the layer of ε_H) are essentially lower than that in structures 1 and 3 (starting by the layers of ε_L). Thus, the value of first layer's permittivity determines the value of optical field within the structure. In all considered structures amplitude of electric field decays starting from the illuminated interface towards the end of the structure, though non-monotonically for the structures having ε_L at the end of the structure (structures 2 and 3). At permittivity lower contrast, the slope of oscillating field envelope decreases in all DBRs that indicates an increase in optical field penetration depth into the structure.

In structures 2 and 4 of Fig. 4, which are started by the layer of high permittivity, the illuminated boundary of the first layer is located at the node of electric field amplitude, while in structures 1 and 3, this boundary is located at the antinode of the field amplitude. As a consequence, in these structures, the high intensity incident field at the illuminated boundary of the first layer can cause damage of a mirror [32].

From the considered types of possible DBRs, structure 4 is an optimal one from the point of view of the highest reflectance (at the same number of layers) and field amplitude distribution (the field in the structure is the lowest and the illuminated boundary of the first layer is located at the node of the field amplitude). As the considered structures and surrounding media are lossless, then the power flow density P is constant inside and outside of the structures (Figs. 4 and 5). The obtained optical field distributions are the result of correct wavelength-scale boundary problem solution, which will be useful in explaining loss impact on reflectance of different types of lossy DBRs.

The non-monotonic behaviour of internal electric field in structures 2 and 3 (Fig. 4) can become a symmetrical field distribution within the structure at definite number of layers. By having symmetrical structure with ε_L outermost, a full transmission is observed (Fig. 5).

At permittivity lower contrast of DBR layers, the similar field distribution is observed at greater number of layers [Fig. 5(b)]. This type of symmetrical field distribution of "butterfly" pattern is observed for transparent DBR structures having ε_L outermost at definite number of layers. Similar "butterfly" pattern for internal electric field amplitude in edge-emitting distributed feedback laser has been obtained by the probability-amplitude method [33].

The relevant conditions of full transparency of DBRs can be obtained from analytical Eqs. (7) and (8). At even number of layers of DBRs, the condition for $R_N \approx 0$ is obtained from Eq. (7)

$$N = \left[\frac{\lg \sqrt{\varepsilon_{sub}} - \lg \sqrt{\varepsilon_1}}{\lg \varepsilon_3 - \lg \varepsilon_2} \right]_{Integer} . \qquad (9)$$

It follows, that R_N can be equal to zero actually for high number of N depending on the permittivity contrast of DBR constituting layers. Transparency is possible only at the difference between the values of ε_{sub} and ε_1 where DBR can be used as an antireflection coating.

At odd number of layers of DBRs, the condition for $R_{N+1} \approx 0$ is obtained from Eq. (8)

$$N = \left[\frac{\lg \varepsilon_2 - \lg(\sqrt{\varepsilon_{sub}}\sqrt{\varepsilon_1})}{\lg \varepsilon_3 - \lg \varepsilon_2} \right]_{Integer} . \qquad (10)$$

The reflectance R_{N+1} can be equal to zero actually for high number of N depending on the permittivity contrast of DBR constituting layers. It is worth to note, that the relation between permitivities of layers and surrounding media should ensure a positive value of N in Eqs. (9) and (10).

The transparency of the DBRs at definite number of layers revealed through the computation of symmetrical field distribution by the MSE is in an excellent agreement with analytical Eqs. (9) and (10), which can be useful in predicting anti-reflecting features of DBRs.

3.2. Lossy DBRs at central wavelength

Since in many devices DBRs are made of semiconductor materials which possess material absorption, then it is expedient to analyse the influence of loss on optical characteristics of different types of DBR structures. Preliminary results of investigation by the MSE have been presented in Ref. 34.

Well-known Eqs. (7) and (8) for DBR reflectance are derived by using the TMM only for lossless DBRs. Direct inclusion of imaginary part of permittivity in these formulae gives completely wrong results for lossy DBRs. Since the

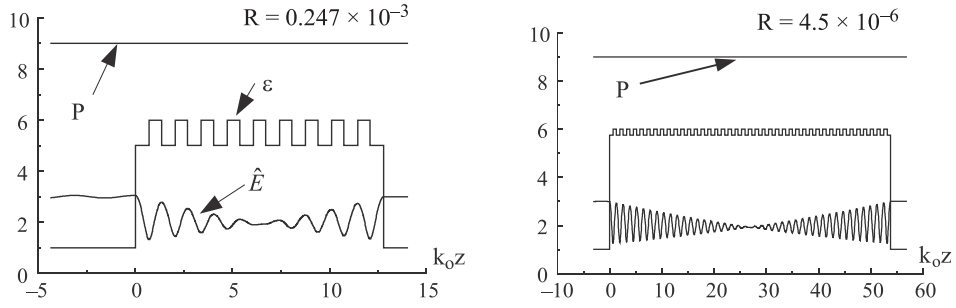

Fig. 5. The permittivity profile, distributions of electric field amplitude $\hat{E}$ and the power flow density P in DBR of the type $\varepsilon_1/(\varepsilon_L/\varepsilon_H)\times N + \varepsilon_L/\varepsilon_1$ at $N = 9.\varepsilon_L = 5, \varepsilon_H = 6$ (a) and at $N = 41.\varepsilon_L = 5.75, \varepsilon_H = 6, \varepsilon_1 = 1$ (b). Incident field comes from the left of structures and has the amplitude E_{inc} = 3 a.u.

thickness of the multilayer structure is not present in these formulae, then absorption which is accumulated along the structure cannot be correctly accounted. It is possible to analyse lossy DBRs by the TMM only through computational multiplication of all matrices describing constituting layers of DBRs through direct inclusion of loss in each layer of the structure [8,11–13,31].

In the present paper, the analysis of optical properties of lossy DBRs is carried out by the MSE. In this case, the 3rd equation of the set of differential Eq. (3) manages the change of power flow density along each layer of a multilayer structure.

The reflectance dependences on the number N of bilayers of structures 1–4 (Fig. 2) at the absence and at the presence of absorption loss $\varepsilon'' = -0.1$ are presented in Fig. 6.

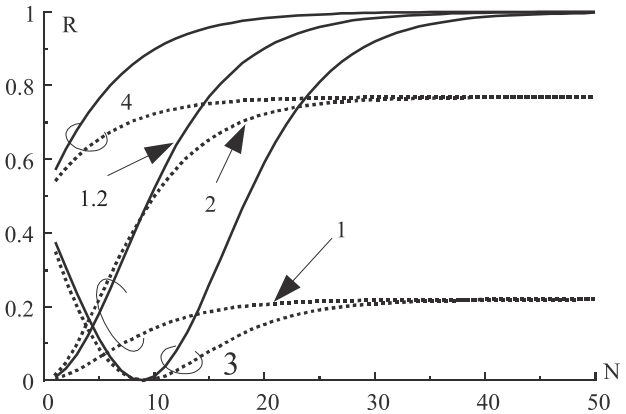

Fig. 6. The reflectances of DBRs 1–4 (Fig. 2) on the number of bilayers at the absence (solid lines) and the presence of loss (dotted lines) $\varepsilon'_L = 5, \varepsilon'_H = 6, \varepsilon_{sub} = \varepsilon_1 = 1, \varepsilon'' = -0.1$.

The presence of loss brings to decrease in reflectance of all considered DBRs for any number of layers. For the structure with loss the condition $R + T + A = 1$ is fulfilled that follows from the energy conservation law. At high enough number of lossy layers, the transmittance $T = 0$ and $R = 1 - A$. Here, the absorptance $A = P_{loss}/P_{inc}$, P_{loss} is the power absorbed in the structure. The power P_{loss} of the wave absorbed in any 1D structure is proportional to the electric field component's intensity $\left|\hat{E}(z)\right|^2$, imaginary part of the permittivity and the length L of the structure, and it is described by [35,36]

$$P_{loss} = \omega\varepsilon_0 \int_0^L \varepsilon''(z)\left|\tilde{E}(z)\right|^2 dz. \qquad (11)$$

According to Eq. (11), in structures 2 and 4, where the electric field envelope is lower [Figs. 4(b) and 4(d)], the presence of loss has brought to the relatively lower decrease in reflectance, than in structures 1 and 3, where the electric field envelope within the structures is higher [Figs. 4(a) and 4(c)].

To have a physical insight into the loss influence on reflective property of DBRs, it is useful to present distributions of the electric field amplitude $\hat{E}(z)$ and the power flow density $P(z)$ in the considered lossy DBR structures. Corresponding distributions at $\varepsilon'' = -0.1$ in all layers of the DBRs are presented in Fig. 7.

In all structures, stepwise diminution of power flow density is stipulated by the oscillating character of electric field amplitude along the structures. In structures 1 and 3, starting by a layer of low permittivity where the envelope of field amplitude is relatively high, higher absorption of the power [$P_{loss} = P(z = 0) - P(z = L)$] is observed [Figs. 7(a) and 7(c)]. In structures 2 and 4, starting by a layer of high permittivity, the envelope of electric field amplitude within the structure is relatively low and consequently absorption of the power is essentially low [Figs. 7(b) and 7(d)]. These structures will be less influenced by loss and again an optimal structure is number 4 with outermost layers of ε_H. DBRs of high permittivity layers outermost are advantageous in efficient operation of surface-normal electro-absorption modulators [37].

3.3. Spectral characteristics of lossy DBRs

Since DBRs possess high reflectance not only at Bragg wavelength (called central wavelenght), but also within some frequency band around it, then it is desirable to investigate the influence of absorption loss on the spectral characteristics of DBRs. The spectral characteristics of the structures in Fig. 2 are calculated by the MSE and they are presented in Fig. 8. The presence of loss brings to the general decrease in reflectance within the frequency band. For struc-

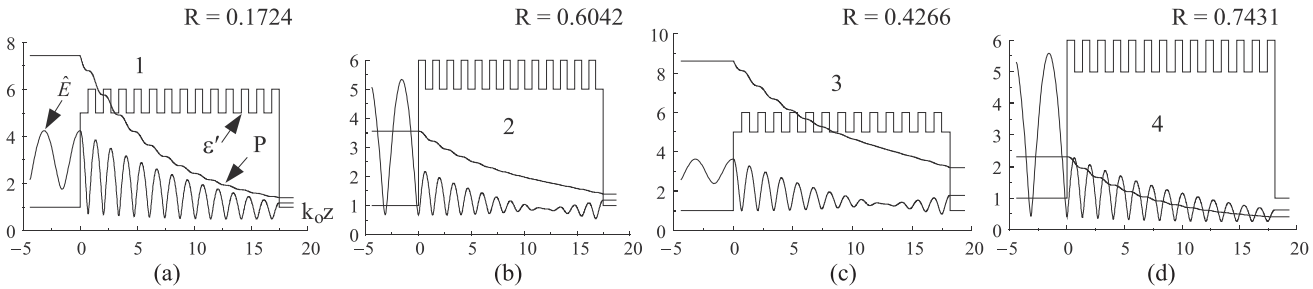

Fig. 7. The permittivity profile, distributions of the electric field amplitude and the power flow density in lossy DBRs of the following alternation of layers: (a) $\varepsilon_1/(\varepsilon_L/\varepsilon_H)\times N/\varepsilon_1$, (b) $\varepsilon_1/(\varepsilon_H/\varepsilon_L)\times N/\varepsilon_1$, (c) $\varepsilon_1/(\varepsilon_L/\varepsilon_H)\times N+\varepsilon_L/\varepsilon_1$ and (d) $\varepsilon_1/(\varepsilon_H/\varepsilon_L)\times N+\varepsilon_H/\varepsilon_1$ at $N = 13$. Corresponding values of the reflectance R are indicated at $\varepsilon'' = -0.1$ in all layers. DBRs are surrounded from both sides by the air $\varepsilon = 1$. Incident field comes from the left of structures and has the amplitude $E_{inc} = 3$ a.u.

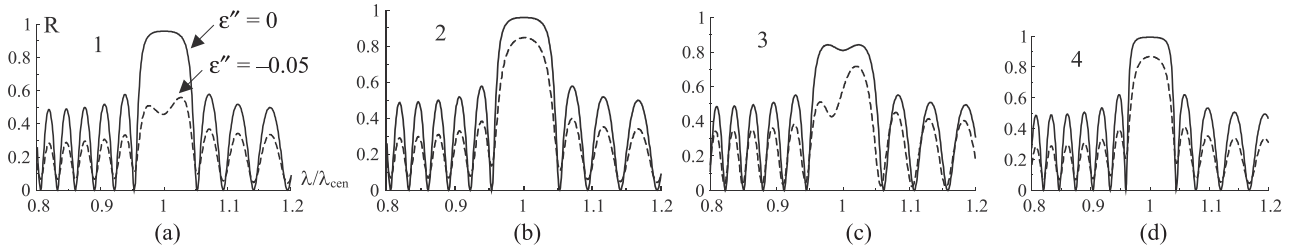

Fig. 8. Spectral characteristic of the structures presented in Fig. 2 with and without loss in the layers at the bilayer number $N = 25, \varepsilon'_L = 5, \varepsilon'_H = 6, \varepsilon_{sub} = \varepsilon_1 = 1$.

tures 1 and 3, the presence of loss brings to a relatively higher decrease in the reflectance within the main frequency band [Figs. 8(a) and 8(c)] and *vice versa* for structures 2 and 4 [Figs. 8(b) and 8(d)]. In the structures with higher envelope of internal optical field amplitude, the influence of loss is stronger. Non-regular behaviour of the reflectance in the main frequency band of structures 1 and 3 is explained by strong impact of loss at central wavelength.

Again, the structure starting by ε_H is more suitable to be served as a reflector by having regular behaviour of reflectance in the central wavelength range and also by having comparatively small influence of absorption loss on its reflectance.

4. Conclusions

In the present paper, the problem of normal incidence of plane electromagnetic wave on lossless and lossy DBRs is analysed in details by the MSE. Apart from reflective characteristics of DBRs, distributions of electric field amplitude and power flow density within the DBR structures are obtained by the MSE. The knowledge of electric field distribution within DBRs is especially useful in understanding reflective peculiarities of different types of DBRs. Performed analysis showed that DBRs starting by a quarter-wave layer of high permittivity provide the highest reflectance.

Specific DBRs possessing zero reflectance at the definite number of layers are investigated. Analytical conditions of transparency of these DBRs are obtained and presented. Electric field distribution within the transparent DBRs is symmetric and has a "butterfly" pattern. Transparent DBR structures are promising candidates for application in wide--band amplifying structures [38] and in structures of nonlinear limiters [39].

The presence of absorption loss in DBR structures brings to decrease in their reflectance at any number of layers. DBRs starting by a quarter-wave layer of high permittivity preserve the highest reflectance even in the presence of absorption loss in constituting layers of the structure. The physical explanation is comparatively low amplitude of electric field pattern in this type of DBR structures opposed to DBRs starting by a quarter-wave layer of low permittivity. The lower the amplitude of electric field within DBR, the lower an absorption loss in it. Moreover, in DBRs starting by a quarter-wave layer of high permittivity, the node of standing wave pattern of electric field is located at the illuminated boundary of the first layer which makes this type of DBR structures to be relatively steady to high intensity optical radiation. Thus, DBRs starting by a quarter--wave layer of high permittivity are optimal reflectors providing also regular behaviour of reflectance in the central wavelength range.

Though in the present work investigations are carried out for the model values of layers' permittivity, proceeding from the universality of the considered electrodynamical models, all obtained regularities will be applicable for any dielectric or semiconductor DBR structures.

Though in the present paper classical DBRs with abrupt interfaces have been considered, any other type of graded interfaces of constituting layers is possible to analyse by the MSE.

Acknowledgements

This work was supported by the Swiss National Science Foundation JRP IB7320-111057/1, Armenian National Educational Fund grant EN-elec-1150 and partly by the Armenian State Budget project No. 230. The authors thank also COST Action MP0702 "Towards functional sub-wavelength photonic structures" for stimulating discussions.

References

1. K. Iga, "Surface emitting laser – its birth and generation of new optoelectronics field", *IEEE J. Sel. Top. Quant.* **6**, 1201–1215 (2000).
2. K.D. Choquette and H.Q. Hou, "Vertical-cavity surface emitting lasers: moving from research to manufacturing", *IEEE Proc.* **85**, 1730–1739 (1997).
3. E.F. Schubert, N.E.J. Hunt, J.M. Roger, M. Micovic, and D.L Miller, "Temperature and modulation characteristics of resonant-cavity light-emitting diodes", *J. Lightwave Technol.* **14**, 1721–1729 (1996).
4. D. Delbeke, R. Bockstaele, P. Bienstman, and R. Baets, "High-efficiency semiconductor resonant-cavity light-emitting diodes: A review", *IEEE J. Sel. Top. Quant.* **8**, 189–206 (2002).
5. J.P. Kim and A.M. Sarangan, "Simulation of resonant cavity enhanced (RCE) photodetectors using the finite difference time domain (FDTD) method", *Opt. Express* **12**, 4829–4834 (2004).

6. T.H. Stievater, W.S. Rabinovich, P.G. Goetz, R. Mahon, and S.C. Binari, "A surface-normal coupled-quantum-well modulator at 1.55 μm", *IEEE Photonic. Tech. L.* **16**, 2036–2038 (2004).
7. H. Liu, Ch.Ch. Lin, and J.S. Harris, Jr., "High-speed, dual--function vertical cavity multiple quantum well modulators and photodetectors for optical interconnects", *Opt. Eng.* **40**, 1186–1191 (2001).
8. P. Yeh, *Optical Waves in Layered Media*, N.Y.: Willey & Sons, 1988.
9. A.V. Vinogradov and Ya. Zeldovich, "X-ray and far UV multilayer mirrors: Principles and possibilities", *Appl. Optics* **16**, 89–93 (1977).
10. P. Bienstman, R. Baets, J. Vukusic, A. Larsson, S.A. Riyopoulos, J.F.P. Seurin, and S. L. Chuang, "Comparison of optical VCSEL models on the simulation of oxide-confined devices", *IEEE J. Quantum Elect.* **37**, 1618–1631 (2001).
11. M. Born and E. Wolf, *Principles of Optics*, Pergamon, Oxford, 1975.
12. O.S. Heavens, *Optical Properties of Thin Solid Films*, New York, Dover Publications Inc., 1991.
13. H.A. Macleod, *Thin-Film Optical Filters*, Bristol, Institute of Physics Publishing, 2001.
14. D.I. Babic and S.W. Corzine, "Analytic expressions for the reflection delay, penetration depth, and absorptance of quarter-wave dielectric mirrors", *IEEE J. Quantum Elect.* **28**, 514–524 (1992).
15. O. Arnon and P. Baumeister, "Electric field distribution and the reduction of laser damage in multilayers", *Appl. Optics* **19**, 1853–1855 (1980).
16. K. Ohta and H. Ishida, "Matrix formalism for calculation of electric field intensity of light in stratified multilayered films", *Appl. Optics* **29**, 1952–1959 (1990).
17. H.V. Baghdasaryan and T.M. Knyazyan, "Problem of plane EM wave self-action in multilayer structure: an exact solution", *Opt. Quant. Electron.* **31**, 1059–172 (1999).
18. A. Yariv and P. Yeh, *Optical Waves in Crystals*, John Wiley & Sons. Inc., 1984.
19. B.G. Kim and E. Garmire, "Comparison between the matrix method and the coupled-wave method in the analysis of Bragg reflector structures", *J. Opt. Soc. Am.* **A9**, 132–136 (1992).
20. N. Matuschek, F.X. Kartner, and U. Keller, "Exact coupled-mode theories for multilayer interference coatings with arbitrary strong index modulation", *IEEE J. Quantum Elect.* **33**, 295–302 (1997).
21. M.C. Parker, R.J. Mears, and S.D. Walker, "A Fourier transform theory for photon localization and evanescence in photonic bandgap structures", *J. Opt. A-Pure Appl. Opt.* **3**, S171–S183 (2001).
22. F. De Leonardis, V.M.N. Passaro, and F. Magno, "Improved simulation of VCSEL distributed Bragg reflectors", *J. Comput. Electron.* **6**, 289–292 (2007).
23. S.W. Corzine, R.H. Yan, and L.A. Coldren, "A Tanh substitution technique for the analysis of abrupt and graded interface multilayer dielectric stacks", *IEEE J. Quantum Elect.* **27**, 2086–2090 (1991).
24. A. Taflov and S.C. Hagness, *Computational Electrodynamics: The Finite-Difference Time-Domain Method*, Artech House, Boston, 2000.
25. H.V. Baghdasaryan, "Method of backward calculation", in *Photonic Devices for Telecommunications: How to Model and Measure*, pp. 56–65, edited by G. Guekos, Springer--Verlag, 1999.
26. H.V. Baghdasaryan and T.M. Knyazyan, "Method of single expression – advanced powerful tool for computer modelling of wavelength scale nonuniform frequency-selective 1D photonic structures", *ICTON 2002*, *Conf. Proc*., Poland, Th. C.5, 157–162 (2002).
27. H.V. Baghdasaryan and T.M. Knyazyan, "Method of single expression – an exact solution for wavelength scale 1D photonic structures' computer modelling", *Proc. SPIE* **5260**, 141–148 (2003).
28. H.V. Baghdasaryan and T.M. Knyazyan, "Modelling of strongly nonlinear sinusoidal Bragg gratings by the method of single expression", *Opt. Quantum Elect.* **32**, 869–883 (2000).
29. H.V. Baghdasaryan and T.M. Knyazyan, "Simulation of amplifying phase-shifted Bragg gratings by the method of single expression", *Opt. Quantum Elect.* **35**, 493–506 (2003).
30. M. Midrio, "Shooting technique for the computation of plane-wave reflection and transmission through one-dimensional nonlinear inhomogeneous dielectric structures", *J. Opt. Soc. Am.* **B18**, 1866–1871 (2001).
31. H.M. Liddell, *Computer-Aided Techniques for the Design of Multilayer Filters*, Adam Hilger Ltd., Bristol, 1981.
32. J.H. Apfel, "Optical coating design with reduced electric field intensity", *Appl. Opt.* **16**, 1880–1885 (1977).
33. G.B. Morrison and D.T. Cassidy, "A probability-amplitude transfer-matrix method for calculating the distribution of light in semiconductor lasers", *IEEE J. Quantum Elect.* **39**, 431–437 (2003).
34. H.V. Baghdasaryan, T.M. Knyazyan, and R.I. Simonyan, "Optical characteristics of distributed Bragg reflectors by taking into account material loss in layers", *ICTON 2005*, *Conf. Proc*., Barcelona, 347–350 (2005).
35. H. Puschner, *Heating with Microwaves. Fundamentals*, *Components and Circuit Technique*, Philips Technical Library, 1966.
36. L.D. Landau and E.M. Lifshitz, *Electrodynamics of Continuous Media*, Pergamon Press Ltd., 1984.
37. H.V. Baghdasaryan, T.M. Knyazyan, A.S. Berberyan, T.T. Hovhannisyan, and M. Marciniak, "Numerical analysis of impact of DBRs' outermost layers on optical characteristics of a surface-normal electro-absorption modulator by the method of single expression", *Proc. 11th Int. Conf. on Transparent Optical Networks – ICTON 2009*, IEEE Catalogue No. CFP09485 IEEE, Azores, Tu.C1.4 (2009).
38. H.V. Baghdasaryan, T.M. Knyazyan, and T.H. Baghdasaryan, "Numerical model of new type of DFB SOA on uniform DBR structure completely transparent at Bragg wavelength", *European Semiconductor Laser Workshop 2008*, Eindhoven, 13 (2008).
39. D.E. Pelinovsky, J. Sears, L. Brzozowski, and E.H. Sargent, "Stable all-optical limiting in nonlinear periodic structures. I: Analysis", *J. Opt. Soc. Am.* **B19**, 43–53 (2002).